MARINE ROBOTS

Abyssal Benthic Rover, an autonomous vehicle for long-term monitoring of deep-ocean processes

K. L. Smith Jr.[1]*, A. D. Sherman[1], P. R. McGill[1], R. G. Henthorn[1], J. Ferreira[1], T. P. Connolly[2], C. L. Huffard[1]

The deep-ocean carbon cycle is poorly quantified. An abyssal benthic rover was developed to make long time-series measurements of seafloor processes related to organic carbon remineralization and sequestration. Benthic Rover II (BR-II) is an autonomous dual-tracked vehicle that measures bottom water temperature and oxygen concentration, current velocity, and sediment community oxygen consumption (SCOC; respiration). BR-II is programmed to transit with low surface-contact pressure across the seafloor, photograph bottom conditions, and stop regularly to occupy respirometer incubation sites, with deployment periods up to 1 year. Now, continuously operational at a 4000-m station in the northeast Pacific over 5 years, substantial weekly, seasonal, annual, and episodic events have been recorded, which are critical to assessing the deep-ocean carbon cycle. There was a significant increase in phytodetritus cover ($P < 0.01$) arriving on the seafloor from the overlying water column between 2015 and 2020 that was negatively correlated with bottom water dissolved oxygen concentration ($P < 0.01$). Over the continuous 5-year monitoring period from November 2015 to November 2020, SCOC was positively correlated with phytodetritus cover ($P < 0.01$) and increased significantly from 2015 to 2020 ($P < 0.01$). These results show important influences of biological processes on the carbon cycle. The demonstrated success of BR-II now creates opportunities to expand the long-term monitoring of the deep sea to resolve the coupling of water column and benthic processes key to understanding the oceanic carbon cycle on a planet engulfed in a changing climate.

INTRODUCTION

Extreme environments on Earth are understudied compared with extraterrestrial areas in our solar system. However, the influence of the deep ocean (>2000 m depth) on our lives on Earth will likely have a far greater impact than outer space in our lifetime. The great expanse of the deep ocean covers more than 65% of the globe (*1*) and is very important in the global carbon cycle now heavily influenced by increasing carbon dioxide emissions and resulting changing climate (*2*). To understand current conditions, and model future changes in the carbon cycle (*3*–*7*), including the ocean's capacity to absorb atmospheric carbon dioxide (*8*), it is necessary to quantify the export of particulate carbon produced in the surface waters to the deep ocean and its sequestration there. However, the high hydrostatic pressure, cold temperature, lack of ambient light, and corrosive nature of seawater present major obstacles to long-term monitoring of deep-ocean processes essential in resolving the oceanic carbon cycle. Instrumentation is now being deployed for long-term observations and measurements of the deep-sea floor [Table 1; (*9*–*12*)].

Here, we report the successful, sustained performance of a fully autonomous bottom-transiting instrument, which images the deep-ocean floor and measures carbon remineralization (the breakdown of organic matter into simpler components including CO_2) over continuous year-long periods at 4000 m depth (Movie 1). Such measurements are critical for quantifying carbon sequestration in the deep ocean [e.g. (*13*)].

The instrument

Benthic Rover II (BR-II) is an autonomous bottom-transiting vehicle capable of long-term monitoring of seafloor processes, which replaces a stationary, lander-based respirometry system that was restricted to several-day deployments (*14*, *15*). Development of this vehicle spans ~25 years, including both successes and failures (*9*, *10*, *16*), to ultimately reach a reliable long-duration instrument, BR-II (Fig. 1). It is now routinely deployed to 4000 m depth in the eastern North Pacific [Station M; (*17*)].

BR-II has been designed to handle the cold, corrosive, and high-pressure conditions of the abyssal benthos and transits with low surface-contact pressure across a soft-sediment seafloor. The instrument platform is 2.6 m long, 1.7 m wide, and 1.5 m high and designed for deployments to 6000 m depth. The structural framework of the vehicle is constructed of corrosion-resistant titanium and plastic components (Fig. 1). The vehicle propulsion system consists of two 46-cm-wide polyurethane lugged tracks driven by two brushless motors mounted in pressure-compensated oil-filled housings. Vehicle buoyancy is composed of 18 blocks of syntactic foam and four bored prolate spheroid syntactic floats, all with a 6-km-depth rating (Fig. 1). A cylindrical steel ballast weight (113 kg) is suspended beneath the bed of the vehicle between the tracks. BR-II with ballast weighs 1814 kg in air and 68 kg in seawater. When deployed, the track footprint of the vehicle (0.94 m^2) has a low surface-contact pressure (72 kg m^{-2}), which prevents the platform from settling into the sediment and creates only light track marks on silty-clay sediment during transits. A sling bearing the weight of the ballast is attached to lever-arm mechanisms secured by dual redundant burn-wire loops. An acoustic command from a shipboard transmitter on the surface above initiates the release of the ballast weight sling by galvanic corrosion of a burn-wire. On release of the ballast, the instrument has a positive buoyancy of 45 kg. Changes in vehicle buoyancy due to water density at depth and water absorption into the syntactic foam were calculated to be less than 1% (note S1).

BR-II is equipped with instrumentation to collect sediment data and measure bottom-water characteristics. A two-dimensional

[1]Monterey Bay Aquarium Research Institute, Moss Landing, CA, USA. [2]Moss Landing Marine Laboratories, San José State University, Moss Landing, CA, USA.
*Corresponding author. Email: ksmith@mbari.org

Table 1. Deep-sea bottom crawlers for imaging the seafloor and measuring fluxes across the sediment-water interface.

Benthic crawler	Autonomous	Cabled	Years of operation	Depth of operation (m)	Transit camera	Site camera	Location	Bottom water measurements		Seafloor transit imaging			Seafloor fluxes		Reference
								Temperature	Currents	Fluorescence	Structure	Megafauna	Chamber	Micro-O_2 profiler	
Benthic Rover I	X		1996	4100	X	X	NE Pacific	X	X		X	X	X	X	(*9*)
Benthic Rover II	X	X	2011–present	4000	X	X	NE Pacific	X	X	X	X	X	X		(*10*, *16*, *40*)
Tramper	X		2016–present	2500		X	NW Atlantic						X	X	(*12*)
Wally		X	2013–present	890	X		NE Pacific	X	X		X	X		X	(*11*)

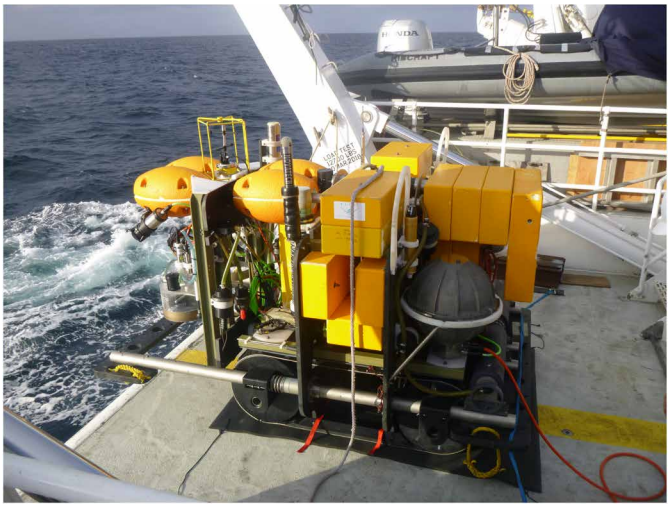

Movie 1. Overview of abyssal BR-II at 4000 m (Station M). Deployment from *RV Western Flyer*, on the seafloor, lowering chambers, transiting, and fluorescence images.

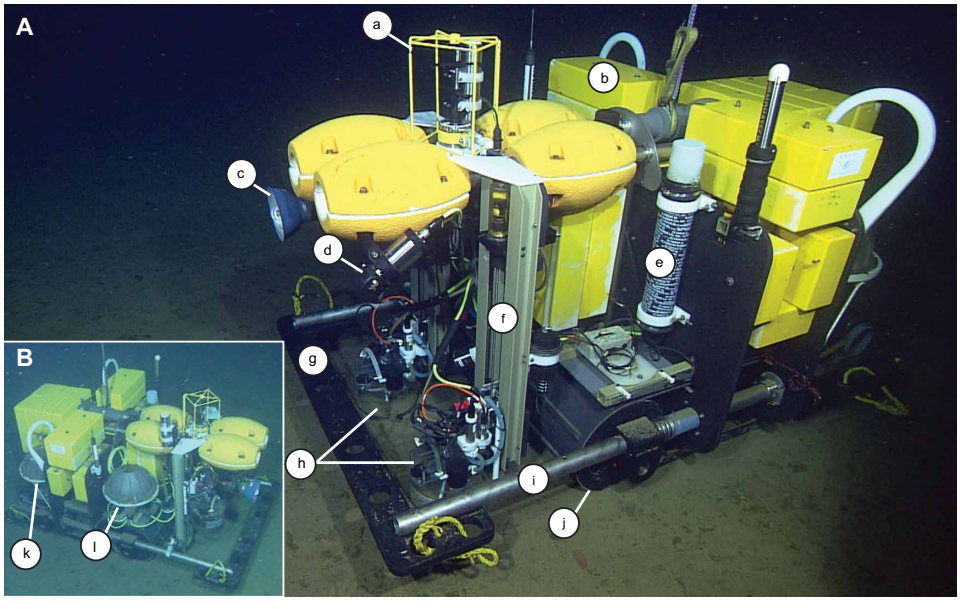

Fig. 1. Abyssal BR-II working on the seafloor at 4,000 m depth. (**A**) BR-II from the port-side perspective. The principal components are the current meter (a), syntactic foam floatation modules (b), strobe (c), transit camera (d), acoustic modem (e), instrument track assembly (f), high-density polyethylene platform (g), respirometer chambers (h), titanium frame (i), and tread (j). (**B**) BR-II from the starboard-side perspective showing one of the titanium battery spheres (k) and the titanium controller sphere (l).

acoustic current meter (Falmouth Scientific, Inc., model 2D-ACM) is mounted on the top of the vehicle to measure horizontal current speed and direction. The front platform of BR-II has two vertically mounted instrument racks located port and starboard (Fig. 1). Critical to the mission of the BR-II is measuring respiration (oxygen consumption) of the sediment community to estimate organic carbon remineralization (*18*). A respirometer chamber is mounted on each rack and moves up and down on a carriage driven by a lead screw geared to a brushless dc motor. The acrylic cylindrical respirometer chambers are 30 cm in diameter and 20 cm high with a Teflon-coated titanium knife edge attached to the bottom rim. In the center of each chamber is a stirrer to circulate the water continuously during incubations and prevent stratification. The oxygen concentration in each chamber is measured by an optode (Aanderaa, model 3830). Two externally mounted optodes provide reference measurements of oxygen and temperature in the surrounding ambient water. Each respirometer has two hydraulically actuated valves that open when the chambers are inserted into the sediment, to prevent a bow wave, and then close to seal during incubations. Two video cameras (Nova from Insite Pacific) are directed at the sediment surface where the port and starboard chambers are inserted. A 5-megapixel (MP) digital survey camera (Prosilica, model GC2450) is mounted on the front port side of the vehicle to capture still color images of the seafloor (fig. S1). Illumination for this camera system is provided by a 250 W-s xenon strobe (Sea & Sea, model YS-250Pro) mounted on the starboard side of BR-II. In addition, a fluorescence imaging system indicates the presence of chlorophyll and phycoerythrin in detrital matter arriving on the seafloor (fig. S1). The seafloor is illuminated by a blue light-emitting diode (475 nm) blocked by a long-pass filter (665 nm) and imaged by a 1.4-MP monochrome camera (model GC1380, Prosilica Inc., Burnaby, British Columbia, Canada) (Fig. 1). While BR-II is deployed autonomously, communication to the ocean surface is conducted through a redundant pair of acoustic modems (Teledyne Benthos, model ATM-887). The vehicle sends status messages about its performance upon request from a surface ship or Wave Glider [Liquid Robotics; (*19*)], which allows for geolocation (*20*). This communication link is also used to release the ballast weight. Two 10-kWh lithium batteries to power BR-II and control electronics are housed in three 43-cm-diameter, spherical titanium pressure housings located forward (electronics) and aft (two for batteries) on the vehicle (Fig. 1).

Energy usage by the BR-II is dominated by the control computer and its peripheral interface boards (58% of the total energy), which must be awake for 2 min of every 15 min to read the oxygen optodes and execute the mission script. The next largest consumer is instrumentation (35%), which includes cameras, lights, and other sensors. Unexpectedly, BR-II electromechanical actuators, which include propulsion motors, rack insertion motors, and chamber valve pumps, consume the least amount of energy (7%) due to their extremely low duty cycle. BR-II can operate for 12.6 months before its batteries are depleted, so there are typically only a few weeks of energy remaining when the vehicle is recovered.

Deployment and mission

BR-II is deployed from a surface ship and free-falls through the water column, taking 2 hours to sink 4000 m to the seafloor. After landing, BR-II surveys sediment and bottom-water conditions at preprogrammed intervals as it transits the seafloor.

A typical mission starts with BR-II transiting from the landing site to a fresh undisturbed incubation site. After landing, BR-II senses the bottom current at 20-min intervals (six measurements per interval), waiting up to 12 hours (average of 5 hours) for a favorable current direction before moving 10 m (100 cm/min) either up or across current to avoid sediment resuspension at the first measurement site. On arrival, there is a pause in operations to allow ambient environmental conditions to stabilize. After this period, the sediment directly in front of the vehicle is imaged with the fluorescence system (fig. S1), after which the two respirometer chambers are slowly lowered independently into the sediment. Each chamber encloses 730 cm^2 of sediment surface to a depth of 2 to 6 cm. Change in oxygen concentration in the overlying chamber water is then measured by optodes every 15 min over the preprogrammed duration of incubation (48 hours). Video cameras capture still frames of the chambers before and after insertion into the sediment (fig. S1). These images provide a measure of the chamber insertion depth into the sediment and also record enclosed sediment structures and fauna. On completion of the first incubation, the chambers are raised and BR-II moves up or across current to the next incubation site, taking 10 photos during the 10-m transit (fig. S1). This cycle of a 2-day incubation following a 10-m transit is repeated over the duration of each deployment. BR-II maintains a constant compass heading to avoid crossing its own tracks and sampling in previously disturbed areas. A Wave Glider transits the surface waters over the BR-II deployment site quarterly to acoustically interrogate the instrument and receive status updates and sample data, which are transmitted via satellite to a shore station. BR-II is recovered after each 12-month deployment and serviced on board the ship in less than 48 hours before being redeployed for another year.

Deployment site

During development and operation, BR-II has been deployed for the past 10 years at a long time-series station (Station M) in the eastern North Pacific located 225 km off the coast of central California at 4000 m depth (*21*). The seafloor at this site has a vertical relief of <100 m over an expanse of 100 km^2 with few obstacles across the level terrain. This station is situated in the productive California Current upwelling region, where sinking particulate organic carbon reaches the silty-clay sediment and sustains deep-ocean communities. These fluxes have markedly increased over the past decade of this 32-year time-series study, with large episodic events accounting for an increasing fraction of yearly food supply (*13*, *17*). Monitoring the impact of such episodic events on the oceanic carbon cycle, including remineralization and sequestration at the seafloor, is now possible with the continuous measurements provided by the development of BR-II.

RESULTS

Instrument performance

The performance of BR-II was evaluated using four criteria: distance traveled, chamber measurement success, transit images, and current meter measurements. Distance traveled on 12 deployments from May 2011 to November 2020 ranged from 0 m in 2015 to 1640 m in 2020 (Table 2). The percent of expected-to-actual distance traveled ranged from 0 to 98.5% (Fig. 2A). The success of the port and starboard chamber measurements was highly variable in the first 5 years of operation but then became consistently high, between 96 and 100% in the last 4 years (Fig. 2B). The volume of overlying water in both chambers was consistent with mean values per deployment of 10.1 to 11.1 liters in the starboard chamber and 10.4 to 10.9 liters in the port chamber (Table 2). For the first portion of the time series, through November 2015, the number of transit images was low, ranging from 0 to 839 (Table 2), because of shorter deployment periods during development. Beginning in November 2015, with the instrument newly capable of annual deployments, the number of transit images rose from 1520 to

Table 2. BR-II performance over 12 deployment periods from May 2011 to October 2020 at Station M. Recorded parameters are distance traveled, number of chamber measurements (port and starboard), mean chamber volume (port and starboard), number of transit images, number of current meter measurements, and overall percent performance (actual divided by expected × 100). Dash entries indicate no measurement.

Deploy date	Recover date	Distance traveled (m)	Chamber readings, port (#)	Chamber readings, starboard (#)	Chamber volume average, port (liter)	Chamber volume average, starboard (liter)	Transit images (#)	Current meter readings (#)	Overall performance (%)
5/21/2011	11/16/2011	160	0	13	–	10.9	115	350736	46.9
11/20/2011	6/11/2012	870	84	86	10.8	10.6	839	1526042	97.3
6/13/2012	11/14/2012	680	59	68	10.4	10.2	641	1167223	95.6
11/15/2012	6/17/2013	210	17	15	11.0	10.9	194	380074	64.0
6/18/2013	4/3/2014	10	0	0	–	–	9	3333	0.4
10/11/2014	6/18/2015	1030	70	0	10.8	–	25	1404299	52.6
6/20/2015	11/6/2015	0	0	0	–	–	0	0	0.0
11/8/2015	11/9/2016	1590	158	64	10.9	11.1	1590	2082070	86.2
11/12/2016	11/9/2017	1590	157	155	10.9	11.0	1590	2051076	98.8
11/11/2017	10/17/2018	1520	151	150	10.9	10.9	1520	1879246	99.2
10/19/2018	10/17/2019	1570	157	157	10.6	10.8	1570	1998232	98.8
10/19/2019	10/28/2020	1640	162	159	10.6	10.8	1640	2067996	98.6

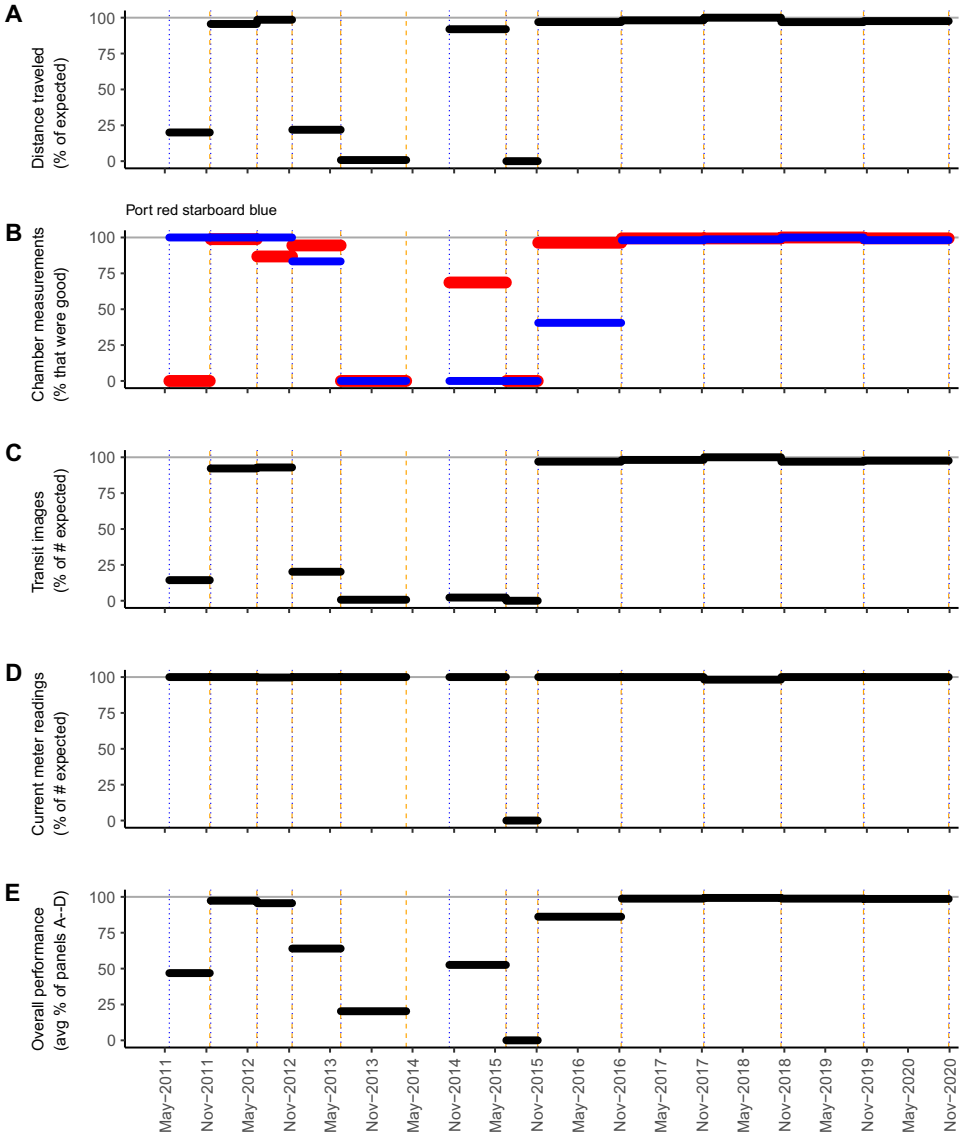

Fig. 2. Abyssal BR-II in situ performance (actual ÷ expected × 100). (**A**) Distance traveled on seafloor transits. (**B**) Chamber measurements of SCOC. (**C**) Transit images. (**D**) Current meter readings. (**E**) Overall performance [average of (A) to (D)]. Vertical dashed lines show dates of deployment (blue) and recovery (orange).

1640 in 2020. The percent success rate increased over the time series, reaching 100% in 2018 (Fig. 2C). The current meter worked well, averaging 12,450 measurements per site on every deployment (Fig. 2D). With the exception of two system failures in 2013 and 2015 due to electronic component and memory card failures, respectively, the current meter recorded from 1.16×10^6 measurements in 2012 to 2.08×10^6 measurements in 2016 (Table 2). The success rate routinely reached 100%, with only two instances recording lower (Fig. 2D).

The overall performance of BR-II using transit distance, chamber measurement success, transit images, and current meter function was highly variable from 2011 to November 2016 (0 to 97.3% success; Fig. 2E). Low success in 2013 and 2014 was due to electronic component failures, and in 2015 due to a failure in the controller's main system flash memory card. BR-II was taken ashore for refurbishment between May and November 2014. From November 2016 to 2020, the performance success was consistently above 98% (98.6 to 99.2%; Table 2). The current success rate is attributed to diligent tracking of every component and keeping extensive prelaunch and postrecovery checklists for maintenance periods at sea. Considering that BR-II is operating in an extreme environment for year-long periods on the deep-sea floor, its development has now reached a very dependable plateau of success.

Measurements

Bottom water characteristics remained relatively stable over the entire deployment period (Fig. 3). Temperature, averaged weekly, had a mean of 1.5 ± 0.0009°C and was consistent throughout the time series (Fig. 3A). Bottom water dissolved oxygen concentration was more variable, ranging from 128.5 to 143.2 µmol with a mean of 136.1 ± 2.3 µmol (Fig. 3B). Noticeable decreases in dissolved oxygen during summer/fall 2012 and spring/summer 2020 coincided with peaks in phytodetrital percent cover and fluorescence on the seafloor (Fig. 3, D and E). However, these periodic decreases rebounded back up afterward. Overall, there was a significant decreasing trend in dissolved oxygen from 2015 to 2020 ($P < 0.01$), following the long-term trend over the 30-year time series at Station M (*17*).

Bottom current over the time series reflected the low-energy, silty-clay sediment environment, with a peak speed of 10.23 cm s^{-1} reached in April 2012 (Fig. 3C). Mean current speed was 2.2 ± 1.31 cm s^{-1}. Mean current velocities (vector averages) over each deployment from 2011 to 2020 had a magnitude that ranged from 2.32 cm s^{-1} for the deployment starting in November 2012 down to 0.09 cm s^{-1} for the deployment starting in November 2017 (Fig. 3C). The mean current velocity for the entire time series had a magnitude of 0.05 ± 0.10 cm s^{-1}. Mean velocity is more relevant to net movement of water, whereas mean speed may be more relevant for sediment resuspension. Current direction was highly variable with the prevailing current toward the second and third quadrants, with mean current direction ranging from 74.1 ± 19.3° in 2012 to 303.1 ± 63.3° in 2017. The bottom currents at Station M varied significantly between years (*22*).

Phytodetritus is particulate organic matter that originates as primary production by phytoplankton in surface waters. Large phytodetrital aggregates, or high coverage of diffuse phytodetritus, can be visible in seafloor imagery [e.g., (*23*) and fig. S1]. Percent cover of phytodetritus on the seafloor ranged from 0 to 100% (21% average), exhibiting seasonal peaks in spring, summer, and fall

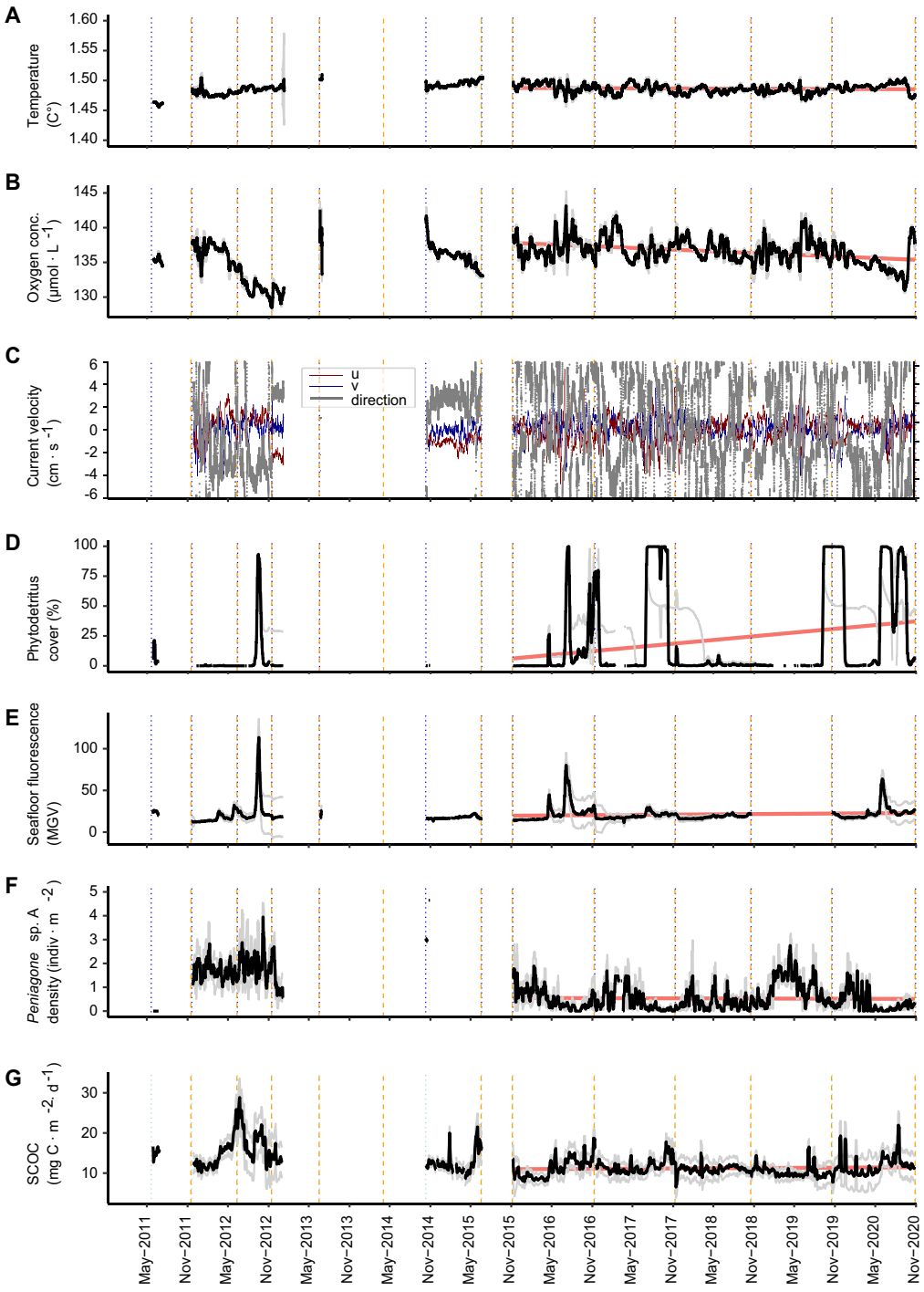

Fig. 3. Time-series measurements using BR-II instrumentation from May 2011 until November 2020 with red trend lines at Station M. (**A**) Bottom water temperature. (**B**) Bottom water dissolved oxygen. (**C**) Bottom current velocity (u and v vectors) and direction. (**D**) Seafloor coverage of phytodetritus. (**E**) Seafloor fluorescence. (**F**) Mobile megafauna density represented by *Peniagone* sp. A. (**G**) SCOC. Gray lines are hourly (A and B) or daily (D to G) means. Black lines are 7-day rolling means. Red trend lines represent the linear regression of the time series from October 2015 to October 2020. Vertical dashed lines show dates of deployment (blue) and recovery (orange).

during the time series. Highs in summer and fall of 2016 were followed by a period of undetectable phytodetritus that lasted until summer 2017, when a long, sustained deposition of phytodetritus occurred through the fall (Fig. 3D). A long period of minimal coverage was recorded from late 2017 until fall 2019, when another sustained peak of phytodetrital material covered the seafloor. Another long period of phytodetrital coverage occurred from spring into fall 2020. There was a significant increase in phytodetrital cover ($P < 0.01$) from November 2015 until November 2020 that was negatively correlated with bottom water dissolved oxygen ($\rho = -0.16$; $P < 0.01$).

Seafloor fluorescence showed spikes in summer of 2012, 2016, and 2020, corresponding with highs in phytodetrital percent cover and indicating enriched material and the presence of chlorophyll, as shown by changes in mean gray values (MGVs) of fluorescence images (11 to 113 MGVs; Fig. 3E). Fluorescence significantly increased

over the 2015-to-2020 period ($P < 0.01$) and was highly correlated with phytodetrital cover ($\rho = 0.70$; $P < 0.01$).

A representative mobile megafauna species, the undescribed elpidiid holothurian *Peniagone* sp. A, was most abundant in summer of 2012, reaching a peak of 4.6 individuals m^{-2}. During the continuous monitoring period between November 2015 and November 2020, abundance ranged from <1 to 3 individuals m^{-2} in spring 2019 (Fig. 3F). The weekly mean abundance through this 5-year period was consistently at 0.8 individuals m^{-2}, with no significant trend over time ($P > 0.05$). Over this period, *Peniagone* sp. A abundance was negatively correlated with phytodetrital cover ($\rho = -0.58$; $P < 0.01$) and seafloor fluorescence ($\rho = -0.54$; $P < 0.01$).

Sediment community oxygen consumption (SCOC) revealed seasonal patterns in remineralization, with highs in spring and fall (Fig. 3G). SCOC reached a high of 34.9 mg C m^{-2} day^{-1} in summer of 2012 and a low of 5.8 mg C m^{-2} day^{-1} in November 2017. Over the full time series, the mean SCOC was 12.1 ± 2.9 mg C m^{-2} day^{-1}. Over the continuous 5-year monitoring period from November 2015 to November 2020, SCOC was positively correlated with seafloor fluorescence ($\rho = 0.53$; $P < 0.01$) and phytodetrital cover ($\rho = 0.49$; $P < 0.01$), with a negative correlation to *Peniagone* sp. A density ($\rho = -0.48$; < 0.01). SCOC increased significantly from 2015 to 2020 ($P < 0.01$), ultimately related to changing surface water conditions and the export flux of organic carbon to the deep ocean [e.g., (*13*, *17*)].

DISCUSSION

The variation in all of the BR-II measurements shows that short-term monitoring efforts are not capable of detecting the underlying fluctuations that drive long-term changes and trends critical to resolving the carbon cycle in the deep ocean. The decreasing trend in bottom water dissolved oxygen is a critical parameter associated with the aerobic remineralization of organic matter. Such a decrease was first noted from bottom water samples taken periodically over 30 years of time-series monitoring at Station M (*17*). This dissolved oxygen decrease could be attributable to a reduction in oceanic ventilation [the transport of water and climatically important trace gases from the surface mixed layer to the ocean interior (*24*)] or increased biological consumption [e.g., (*25*, *26*)]. The continuous monitoring of dissolved oxygen using BR-II now confirms this decreasing trend and reveals a significant correlation with phytodetrital pulses arriving on the seafloor. A further corroboration of biological consumption as the cause of decreasing dissolved oxygen is the significant correlation between SCOC and phytodetrital cover on the seafloor.

The success of BR-II now opens up opportunities to expand the long-term monitoring of the deep sea to resolve the coupling of water column and benthic processes critical to the oceanic carbon cycle. Understanding how carbon flows between deep-sea storage and remineralization processes will be critical to predicting the health and productivity of our planet engulfed in changing climate. Two principal directions of development of BR-II include the expansion of platform measurements and the addition of autonomous coordination with other benthic observatory instrumentation to better resolve carbon cycling in the deep ocean.

Continued development of BR-II

Technological advances in pH sensor development now provide a robust probe suitable for long-term operation at abyssal depths (e.g., PyroScience—optical pH sensor). We are now testing these pH sensors to further instrument BR-II to resolve CO_2, assuming that negligible total alkalinity changes in the chambers, and to provide a more accurate assessment of organic carbon being consumed in the sediments using respiratory quotients (RQs) (CO_2/O_2).

A multiple-coring device has been designed for mounting in front of the BR-II platform to take time-series cores over the course of year-long deployments. These cores will be immediately preserved in situ for later laboratory analyses of carbon content and other sediment properties. This new sampling device and core processing will provide estimates of carbon sequestration for comparison with remineralization rates derived from oxygen consumption and carbon dioxide release.

Real-time communication with BR-II is now possible through modems that acoustically connect the platform to surface Wave Gliders (Liquid Robotics; 18) 4000 m above and then through a satellite link to shore (*20*). This communication network is now functional and becoming more reliable with increased bandwidth (Fig. 4). Transmission of seafloor images and SCOC data to shore in the near future will permit real-time interpretation of seafloor processes, enabling decisions to change the sampling frequency to optimize surveys of episodic events driving possible carbon storage in sediments.

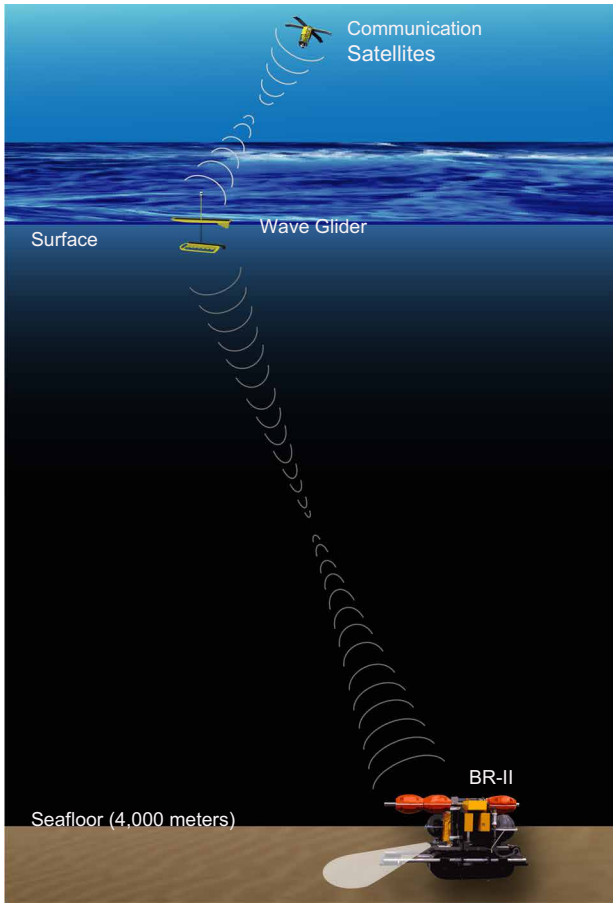

Fig. 4. Depiction of BR-II in action on abyssal seafloor with acoustic communication to a Wave Glider on the surface with continuing link to satellite and back to shore.

Broader time-series networks

Inclusion of BR-II platforms into deep-ocean networks of instruments that survey particle flux will enable researchers to follow carbon photosynthesized in the surface water as it sinks through the water column to the seafloor, where it may be consumed or sequestered in sediments. Autonomous detection of episodic periods when large amounts of particulate matter settle from the overlying water column to the seafloor will soon be used to control and initiate increased sampling frequency of BR-II and other long time-series instruments. If BR-II platforms could be installed at existing long time-series stations at abyssal depths in the North Pacific (three stations) and North Atlantic (four stations) (*27*), then they would provide much-needed resolution of carbon consumption and sequestration to determine the unknown components in oceanic carbon budgets worldwide. One of these long-term sites in the North Atlantic, FRontiers in Arctic marine Monitoring (FRAM), currently has a tracked autonomous vehicle (Tramper) to measure seafloor fluxes (*12*). Tramper has been operational at 2500 m since 2016 (Table 1). A shallower benthic crawler is attached to a cabled observatory (Neptune Canada) monitoring benthic processes in a cold-seep site at 890 m.

BR-II provides data needed to understand how abyssal benthic communities respond to changes in deep-sea carbon cycling, as requested by the Intergovernmental Panel on Climate Change (*8*) and the U.S. Department of the Interior (*28*). Irreversible deep-ocean acidification and deoxygenation are expected on the centennial to millennial scales (*29*). Potential efforts to accelerate storage of atmospheric CO_2 in the ocean (*29*), including in the deep sea (*8*, *30*), are considered and will need in situ data to avoid important ecological risks associated with acidification and eutrophication [eutrophication in the sense of Nixon 1995 "an increase in the rate of supply of organic matter to an ecosystem" in (*31*)]. Results presented here from continuous monitoring of carbon inputs, remineralization rates, and ambient oxygen levels at an abyssal site point to a need to collect these data in other regions and to evaluate whether deep-sea acidification and eutrophication may already be taking place on a large scale. Increasing phytodetritus (surface-derived organic carbon) supply to Station M was positively correlated with remineralization rates (i.e., local biologically mediated CO_2 injection) and negatively correlated with ambient oxygen concentrations, indicating local deoxygenation. Because respiration releases CO_2, which potentially lowers pH (*32*), acidification may have occurred alongside short- and long-term declines in oxygen concentration reported here, including over multiple decades (*17*). Such changes may be expected in other deep-sea areas where carbon export flux appears to be increasing in overlying waters [e.g., fig. S3 in (*18*)].

MATERIALS AND METHODS

Critical components in the operation of BR-II include distance traveled, current measurements, seafloor area imaged, fluorescence, dissolved oxygen, and respiration chamber volume.

Distance traveled

A 1-m section on one track was marked before recording the number of counts on the motor controller resulting in moving 1 m (854 counts). In operation, the motor controller is programmed to move 10 m (10 × 854 counts) at a rate of 854 counts min^{-1}.

Current measurements

The FSI (model 2D-ACM) current meter was factory calibrated. Its main purpose is not precision current speed measurements but to allow BR-II to aim into the current during transits. Current direction derived from the magnetic compass has been corrected for magnetic declination at Station M.

Seafloor area imaged

The transit camera images 3.21 m^2 of the seafloor (fig. S2A). A single observer (K.L.S.) used the open-source software VARS (*33*) to annotate the middle portion of transit color images (40% down from the top and 20% up from the bottom; fig. S2B), with the best lighting conditions, for the area coverage of phytodetritus and the presence of the sea cucumber *Peniagone* sp. A. Percent cover and sea cucumber densities were calculated by dividing the area coverage of phytodetritus and the number of individual *Peniagone* sp. A per image by the area annotated (0.77 m^2).

Fluorescence

MGV of black and white images generated by the fluorescence imaging system was measured to estimate seafloor fluorescence as a possible indicator of chlorophyll concentration. In 2013, a fluorescence reference object (orange fluorescent stick, Sea-Bird Scientific) was attached to the rear surface of BR-II's front cross member. This reference object is visible in the resulting fluorescence images (fig. S1) and was used to evaluate and account for drift in MGV (note S2). Fluorescence generally correlates well with phytoplankton chlorophyll concentration, forming the basis of well-established monitoring of chlorophyll in marine systems (*34*, *35*). Nonetheless, other fluorescent materials in the ocean, including porphyrins found in marine invertebrates (*36*), have spectral properties (*37*–*39*) that might show very weak overlap with the band examined here. A future Rover could certainly include monitoring of a broader range of wavelengths to detect additional organic compounds.

Dissolved oxygen

Aanderaa optodes (model 3830) were two-point calibrated by a manufacturer-authorized repair center or in-house. Temperature of factory and in-house calibrations ranged from 7.06° to 10.08°C. For in-house calibrations, the 100% saturation point was performed in air-bubbled seawater. The 0% point was performed by adding sodium sulfite to seawater until slightly past the point of precipitation (about 10 g $liter^{-1}$). Plotting data from the chamber and reference optodes provided a necessary check of measurement stability over the long-term monitoring period.

Sediment community oxygen consumption

Oxygen concentration in chambers enclosing 730 cm^2 of seafloor surface was measured for 1 min every 15 min during 2-day seafloor respirometry incubations to yield SCOC. The rate of oxygen decline was used to calculate carbon consumption rates based on an RQ of 0.85 (*40*). We chose an RQ of 0.85 to represent a food source of mixed carbohydrate and lipid that best encompasses the sinking particulate matter composition reaching the seafloor at Station M. This value could range from total lipid (0.7) to total carbohydrate (1.0) depending on season, number of trophic transfers, and the rapidity with which the particulate material sinks to the seafloor (*40*).

Respiration chamber volume

The volume of the respirometer chamber for any given incubation was calculated as the sum or difference of two volumes. The first volume is a fixed volume, measured from the top of the titanium knife edge to the chamber's acrylic lid. This volume is known to be 10.21 liter. This volume is then adjusted for each incubation by comparing the sediment level (± cm) in relation to the top of the knife edge. Rulers drawn on the side of the chambers in multiple places enable this measurement from still images taken of chambers lowered into the sediment during each incubation (fig. S1). The second volume component is calculated relative to the top of the knife edge (fig. S1). The volume of that additional seawater in the chamber is calculated with the equation Volume = pi*r^2*L, where r is the radius of the chamber and L is the measured difference between the knife edge and the ruler marking most closely representing the sediment level. If the sediment level is above the knife edge, then this volume is subtracted from the base volume; if the sediment level is below the knife edge, then the additional volume is added to the base volume. The sum or difference yields the total volume of seawater in the chamber for each incubation. The combined mean and variance for chamber volumes for all deployments were 10.8 ± 0.54 liters for the starboard chamber and 10.8 ± 0.4 liters for the port chamber (note S3).

Statistical analysis

Data collected hourly or more frequently (current meter readings, temperature, and oxygen concentration) were averaged to the nearest hour. All other data were originally collected at, or averaged to, the daily scale. These aggregated data were used to calculate 7-day rolling means. Current velocities were smoothed using a low-pass filter with a half-power period of 38 hours. Standard errors of current velocities were calculated using the record length divided by 20 days as effective degrees of freedom. Spearman rank correlation analysis and linear regression were performed on 7-day rolling means of data collected from October 2015 to October 2020, a period with no turnover of individual sensors. All statistical analyses were performed with R (*41*) in RStudio (*42*).

SUPPLEMENTARY MATERIALS

www.science.org/doi/10.1126/scirobotics.abl4925
Figs. S1 and S2
Notes S1 to S3
Reference (*43*)
Movie S1

REFERENCES AND NOTES

1. I. G. Priede, *Deep-Sea Fishes: Biology, Diversity, Ecology and Fisheries* (Cambridge Univ. Press, 2017), p. 492.
2. C. M. Marsay, R. J. Sanders, S. A. Henson, K. Pabortsava, E. P. Achterberg, R. S. Lampitt, Attenuation of sinking particulate organic carbon flux through the mesopelagic ocean. *Proc. Natl. Acad. Sci. U.S.A.* **112**, 1089–1094 (2015).
3. P. Falkowski, R. T. Barber, V. Smetacek, Biogeochemical controls and feedbacks on ocean primary production. *Science* **281**, 200–206 (1998).
4. T. DeVries, F. Primeau, C. Deutsch, The sequestration efficiency of the biological pump. *Geophys. Res. Lett.* **39**, L13601 (2012).
5. D. A. Siegel, K. O. Buesseler, S. C. Doney, S. F. Sailley, M. J. Behrenfeld, P. W. Boyd, Global assessment of ocean carbon export by combining satellite observations and food-web models. *Glob. Biogeochem. Cycles* **28**, 181–196 (2014).
6. P. W. Boyd, H. Claustre, M. Levy, D. A. Siegel, T. Weber, Multi-faceted particle pumps drive carbon sequestration in the ocean. *Nature* **568**, 327–335 (2019).
7. N. Briggs, G. Dall'Olmo, H. Claustre, Major role of particle fragmentation in regulating biological sequestration of CO2 by the oceans. *Science* **367**, 791–793 (2020).
8. IPCC, *IPCC Special Report on Carbon Dioxide Capture and Storage. Prepared by Working Group III of the Intergovernmental Panel on Climate Change*, B. Metz, O. Davidson, H. C. de Coninck, M. Loos, L. A. Meyer, Eds. (Cambridge Univ. Press, 2005), p. 442.
9. K. L. Smith Jr., R. C. Glatts, R. J. Baldwin, S. E. Beaulieu, A. H. Uhlman, R. C. Horn, C. E. Reimers, An autonomous, bottom-transecting vehicle for making long time-series measurements of sediment community oxygen consumption to abyssal depths. *Limnol. Oceanogr.* **42**, 1601–1612 (1997).
10. A. D. Sherman, K. L. Smith Jr., Deep-sea benthic boundary layer communities and food supply: A long-term monitoring strategy. *Deep-Sea Res. II* **56**, 1754–1762 (2009).
11. A. Purser, L. Thomsen, C. Barnes, M. Best, R. Chapman, M. Hofbauer, M. Menzel, H. Wagner, Temporal and spatial benthic data collection via an internet operated deep sea crawler. *Methods iOceanogr.* **5**, 1–18 (2013).
12. F. Wenzhoefer, J. Lemburg, M. Hofbauer, S. Lehmenhecker, P. Faerber. Tramper: An autonomous crawler for long-term benthic oxygen flux studies in remote deep sea ecosystems, in *Proceedings of the OCEANS 2016 MTS/IEEE Monterey* (IEEE, 2016).
13. K. L. Smith Jr., H. A. Ruhl, C. L. Huffard, M. Messie, M. Kahru, Episodic organic carbon fluxes from surface ocean to abyssal depths during long-term monitoring in NE Pacific. *Proc. Natl. Acad. Sci. U.S.A.* **115**, 12235–12240 (2018).
14. K. L. Smith Jr., G. A. White, M. B. Laver, Oxygen uptake and nutrient exchange of sediments measured in situ using a free vehicle grab respirometer. *Deep-Sea Res.* **26A**, 337–346 (1979).
15. K. L. Smith Jr., R. J. Baldwin, Deep-sea respirometry: In situ techniques, in *Polarographic Oxygen Sensors*, E. Gnaiger, H. Forstner, Eds. (Springer-Verlag, 1983), pp. 298–319.
16. P. R. McGill, A. D. Sherman, B. W. Hobson, R. G. Henthorn, K. L. Smith Jr., Initial deployments of the Rover, an autonomous bottom-transecting instrument platform. *J. Ocean Technol.* **4**, 9–26 (2009).
17. K. L. Smith Jr., C. L. Huffard, H. A. Ruhl, Thirty-year time series study at a station in the abyssal NE Pacific: An introduction. *Deep-Sea Res. II* **173**, 104764 (2020).
18. K. L. Smith Jr., H. A. Ruhl, M. Kahru, C. L. Huffard, A. D. Sherman, Deep ocean communities impacted by changing climate over 24 y in the abyssal northeast Pacific Ocean. *Proc. Natl. Acad. Sci. U.S.A.* **110**, 19838–19841 (2013).
19. R. Hine, S. Willcox, G. Hine, T. Richardson, The Wave Glider: A wave-powered autonomous marine vehicle, in *OCEANS 2009* (IEEE, 2009).
20. I. Masmitja, S. Gomariz, J. Del-Rio, B. Kieft, T. O'Reilly, P.-J. Bouvet, J. Aguzzi, Optimal path shape for range-only underwater target localization using a Wave Glider. *Int. J. Robot. Res.* **37**, 1447–1462 (2018).
21. K. L. Smith Jr., E. R. M. Druffel, Long time-series monitoring of an abyssal site in the NE Pacific. *Deep Sea Res. II* **45**, 573–586 (1998).
22. T. P. Connolly, P. R. McGill, R. G. Henthorn, D. A. Burrier, C. Michaud, Near-bottom currents at Station M in the abyssal Northeast Pacific. *Deep-Sea Res. II* **173**, 104743 (2020).
23. D. S. M. Billett, R. S. Lampitt, A. L. Rice, R. F. C. Mantoura, Seasonal sedimentation of phytoplankton to the deep-sea benthos. *Nature* **302**, 520–522 (1983).
24. S. Khatiwala, F. Primeau, M. Holzer, Ventilation of the deep ocean constrained with tracer observations and implications for radiocarbon estimates of ideal mean age. *Earth Planet. Sci. Lett.* **325-326**, 116–125 (2012).
25. S. Schmidtko, L. Stramma, M. Visbeck, Decline in global oceanic oxygen content during the past five decades. *Nature* **542**, 335–339 (2017).
26. K. P. Helm, N. L. Bindoff, J. A. Church, Observed decreases in oxygen content of the global ocean. *Geophys. Res. Lett.* **38**, L23602 (2011).
27. K. L. Smith Jr., M. Messie, A. D. Sherman, C. L. Huffard, B. W. Hobson, H. A. Ruhl, A. Boetius, Navigating the uncertain future of global oceanic time series. *Eos* **96**, (2015).
28. H. Benway, S. Alin, E. Boyer, W.-J. Cai, P. Coble, J. Cross, M. Friedrichs, M. Goñi, P. Griffith, M. Herrmann, S. Lohrenz, J. Mathis, G. McKinley, R. Najjar, C. Pilskaln, S. Siedlecki, R. Smith, "A science plan for carbon cycle research in North American coastal waters" (Report of the Coastal CARbon Synthesis (CCARS) community workshop, August 19–21, 2014, Ocean Carbon and Biogeochemistry Program and North American Carbon Program, 2016), 84 pp.
29. IPCC, Summary for policymakers, in: *Climate Change 2021: The Physical Science Basis. Contribution of Working Group I to the Sixth Assessment Report of the Intergovernmental Panel on Climate Change*, V. Masson-Delmotte, P. Zhai, A. Pirani, S. L. Connors, C. Péan, S. Berger, N. Caud, Y. Chen, L.Goldfarb, M. I. Gomis, M. Huang, K. Leitzell, E. Lonnoy, J. B. R. Matthews, T. K. Maycock, T. Waterfield, O. Yelekçi, R. Yu, B. Zhou, Eds. (Cambridge Univ. Press, in press).
30. Y. Teng, D. Zhang, Long-term viability of carbon sequestration in deep-sea sediments. *Sci. Adv.* **4**, eaao6588 (2018).
31. D. Y. C. Leung, G. Caramanna, M. M. Maroto-Valer, An overview of current status of carbon dioxide capture and storage technologies. *Renew. Sust. Energ. Rev.* **39**, 426–443 (2014).
32. R. A. Feely, S. R. Alin, J. Newton, C. L. Sabine, M. Warner, A. Devol, C. Krembs, C. Maloy, The combined effects of ocean acidification, mixing, and respiration on pH and carbonate saturation in an urbanized estuary. *Estuar. Coast. Shelf Sci.* **88**, 442–449 (2010).

33. B. M. Schlining, N. Jacobsen Stout, MBARI's video annotation and reference system, in *OCEANS 2006* (IEEE, 2006).
34. C. S. Yentsch, D. W. Menzel, A method for the determination of phytoplankton chlorophyll and phaeophytin by fluorescence. *Deep-Sea Res. Oceanogr. Abstr.* **10**, 221–231 (1963).
35. J. Gower, S. King, Validation of chlorophyll fluorescence derived from MERIS on the west coast of Canada. *Int. J. Remote Sens.* **28**, 625–635 (2007).
36. Y. G. Kennedy, Porphyrins in invertebrates. *Ann. N. Y. Acad. Sci.* **244**, 662–673 (1975).
37. P. J. Herring, Porphyrin pigmentation in deep-sea medusae. *Nature* **238**, 276–277 (1972).
38. S. T. Williams, S. Ito, K. Wakamatsu, T. Goral, N. P. Edwards, R. A. Wogelius, T. Henkel, L. F. C. de Oliveira, L. F. Maia, S. Strekopytov, T. Jeffries, D. I. Speiser, J. T. Marsden, Identification of shell colour pigments in marine snails *Clanculus pharaonius* and *C. margaritarius* (Trochoidea; Gastropoda). *PLOS ONE* **11**, e0156664 (2016).
39. C. Martins, A. P. Rodrigo, L. Cabrita, P. Henriques, A. J. Parola, P. M. Costa, The complexity of porphyrin-like pigments in a marine annelid sheds new light on haem metabolism in aquatic invertebrates. *Sci. Rep.* **9**, 12930 (2019).
40. K. L. Smith Jr., C. L. Huffard, A. D. Sherman, H. A. Ruhl, Decadal change in sediment community oxygen consumption in the abyssal Northeast Pacific. *Aquat. Geochem.* **22**, 401–417 (2016).
41. R Core Team, *R: A Language and Environment for Statistical Computing* (R Foundation for Statistical Computing, 2017); https://www.R-project.org/.
42. RStudio Team, *RStudio: Integrated Development for R* (RStudio Inc., 2019); http://www.rstudio.com/.
43. C. Schneider, W. Rasband, K. Eliceiri, NIH Image to ImageJ: 25 years of image analysis. *Nat. Methods* **9**, 671–675 (2012).

Acknowledgments: Many colleagues have greatly contributed to the successful development of BR-II over the long course of this development first including A. Uhlman, R. Baldwin, R. Wilson, R. Glatts, and M. Kirk at Scripps Institution of Oceanography (University of California, San Diego). More recently, J. Ellena, B. Hobson, and L. Bird, along with the remotely operated vehicle pilots K. Brekke, M. Talkovic, D. J. Osborne, and R. Prickett, at MBARI provided viable input to hone the final development process. This contribution was considerably improved by the constructive comments from two anonymous reviewers. **Funding:** This research was initially funded by National Science Foundation (NSF) grant OCE0242472 (2002–2006) to K.L.S. for development of the BR-II at the University of California, San Diego. Remaining NSF funds were then transferred with K.L.S. to the Monterey Bay Aquarium Research Institute as OCE0638505 (2006–2008). BR-II development continued through generous support from the David and Lucile Packard Foundation to K.L.S. from 2007 to present. **Author contributions:** Conceptualization: K.L.S. Methodology: K.L.S., C.L.H., A.D.S., P.R.M., R.G.H., and T.P.C. Investigation: K.L.S., C.L.H., A.D.S., P.R.M., R.G.H., and T.P.C. Visualization: K.L.S., C.L.H., P.R.M., and T.P.C. Funding acquisition: K.L.S. Project administration: C.L.H. and A.D.S. Supervision: K.L.S., A.D.S., C.L.H., and P.R.M. Writing—original draft: K.L.S. and C.L.H. Writing—review and editing: K.L.S., C.L.H., A.D.S., P.R.M., R.G.H., J.F., and T.P.C. **Competing interests:** The authors declare that they have no competing interests. **Data and materials availability:** All data needed to evaluate the conclusions in the paper are present in the paper or the Supplementary Materials.

Submitted 16 July 2021
Accepted 6 October 2021
Published 3 November 2021
10.1126/scirobotics.abl4925

Science Robotics

Abyssal Benthic Rover, an autonomous vehicle for long-term monitoring of deep-ocean processes

K. L. Smith, Jr., A. D. Sherman, P. R. McGill, R. G. Henthorn, J. Ferreira, T. P. Connolly, and C. L. Huffard

Sci. Robot. **6** (60), eabl4925. DOI: 10.1126/scirobotics.abl4925

Science Robotics (ISSN 2470-9476) is published by the American Association for the Advancement of Science. 1200 New York Avenue NW, Washington, DC 20005. The title *Science Robotics* is a registered trademark of AAAS.